Volume 24, No 3 | International Journal of Radiation Research, July 2026

Measurement of equivalent organ doses received by medical personnel during coronary intervention procedures using Geant4 Application for Tomographic Emission (GATE)

H. Mathavan[1,2], S.H. Zuber[1*], M.F. Rizal Abdul Hadi[3], M.S. Ahmad Fadzil[1], A. Sabarudin[1], N.H. Ab. Aziz[3], G. Ramachandran[1]

[1]*Centre for Diagnostic, Therapeutic and Investigative Studies, Faculty of Health Sciences, University Kebangsaan Malaysia, 50300, Kuala Lumpur, Malaysia*

[2]*Department of Diagnostic Radiology, Singapore General Hospital, 169608, Singapore, Singapore*

[3]*School of Physics, University Sains Malaysia, 11800, Penang, MALAYSIA*

► ***Original article***

***Corresponding author:**
Zuber Siti Hajar, Ph.D.,
***E-mail:** hajarzuber@ukm.edu.my*

Received: February 2025
Final revised: November 2025
Accepted: December 2025

Int. J. Radiat. Res., July 2026; 24(3): 641-646

DOI: 10.61186/ijrr.24.3.8

Keywords: *Occupational radiation, coronary angiography, medical personnel, Monte Carlo, GATE.*

ABSTRACT

Background: This study aims to measure the equivalent organ doses received by medical personnel during the coronary intervention procedure using Monte Carlo Geant4 Application for Tomographic Emission (GATE) simulation. ***Materials and Methods:*** The specific dimension of the angiography room was recorded from the Department of Diagnostic Radiology at Singapore General Hospital to generate the angiography room geometry in GATE. ICRP phantom was utilized to represent the medical personnel whereas MIRD phantom was used to represent the patient on the tabletop. Dose received by medical personnel were recorded at anterior posterior (AP) exposure projection at 73 kVp and 350 mAs for all the rooms. ***Results:*** The study revealed variations in the equivalent doses received by medical personnel across different room configurations. The highest dose variation was observed in the right and left lens, with the IR1 exhibiting the greatest exposure. ***Conclusion:*** This highlights the importance of using GATE simulation, as it enables accurate modeling of radiation scattering in various room setups, ensuring precise dose calculations.

INTRODUCTION

Interventional radiology procedures are being increasingly utilized [1, 2] to treat a broad range of diseases, with many now replacing complex surgical procedures [3]. In the medical field, a large amount of ionizing radiation is frequently used to achieve optimal clinical goals with treatments that require radiation [4]. Some patients receive high doses of radiation during diagnosis, treatment, and follow-up, raising particular concerns about the potential for radiation fibrosis syndrome [5, 6]. The United Nations Scientific Committee on the Effects of Atomic Radiation (UNSCEAR) Report 2008 estimated that four billion X-ray examinations were being undertaken per year worldwide. All these procedures must be carried out by medical staff who might become exposed to high levels of radiation.

Medical personnel need to be close to patients during procedures due to the increasing number of projections and the complexity of the procedures. The complexity results in significant potential radiation exposure [7] in the workplace, so appropriate measures must be taken to ensure that actual radiation exposure remains low and does not exceed the permitted limits. Over time, frequent exposure to radiation can lead to a substantial cumulative dose for medical personnel and increase the risk of stochastic effects. These include the probability of cancer and hereditary diseases, as well as deterministic effects involving tissue damage due to radiation. The prolonged exposure to radiation during the procedure can adversely affect the medical personnel involved [8–10].

Monte Carlo methods are powerful tools in radiation studies [11–18], offering detailed and accurate dose calculations for various medical and radiological procedures. They help optimize safety protocols, improve training and education, and contribute to a better understanding of radiation interactions. These methods are also used in research settings to investigate new treatment techniques, evaluate novel imaging protocols, and validate experimental results against theoretical predictions [19–21]. A notable implementation of these methods is the Geant4 Application for Tomographic Emission (GATE) Monte Carlo simulation framework, which is widely used in medical imaging and radiotherapy research [22]. GATE allows the simulation of complex interactions between radiation and matter, supporting the development of new imaging technologies, treatment planning systems, and dose estimation models. By providing precise radiation transport simulations, GATE enhances the accuracy of clinical procedures

[DOI: 10.61186/ijrr.24.3.8]

and facilitates the advancement of personalized medicine. The current work involved measuring the organ equivalent doses received by medical personnel during a coronary intervention procedure using a Monte Carlo GATE simulation. The novelty of this work lies in the development of automated GATE v9.4 command scripts to streamline simulation setups, thus minimizing human error, and the use of SpekPy to generate highly customizable X-ray spectra tailored to complex interventional procedures.

MATERIAL AND METHODS

Generation of geometries in Monte Carlo GATE

For the Monte Carlo simulation, a custom-built personal computer (PC) with an INTEL Core I9 14900K 24 Cores 32 Threads 3.2Ghz LGA1700 Processor was utilized with an Ubuntu 22.04.4 LTS operating system (OS). GATE v9.4 including the Geant4 v11.2.1 and Root v6.28/12 platforms was used to run for the GATE simulation. The angiography room geometry was developed in GATE based on the layout and specifications of the Department of Diagnostic Radiology at Singapore General Hospital, Singapore. This Monte Carlo simulation aimed to closely replicate the real-world environment for accurate modelling and analysis. To ensure the simulation's relevance to clinical practice, coronary intervention procedure was chosen.

Five angiography rooms were generated in Monte Carlo GATE, include IR1, IR3, IR4, IR5 and IR6. In each angiography room, measurements were taken of scattered radiation during the procedure to evaluate radiation exposure patterns. These measurements focused on areas where medical personnel are typically positioned during procedures, providing data to assess the occupational exposure risks. Figure 1 shows angiography room geometries for the GATE simulation. Figure 2 illustrates the position of medical personnel and patient during the intervention procedure.

Utilization of SpekPy to generate energy spectra

In this work, the beam was modelled using SpekPy to generate the spectrum requires for the tube voltage. The specific SpekPy command provided a detailed overview of the configuration and input parameters used to generate the X-ray spectrum.

Measurement of dose in Monte Carlo GATE

The measurement of scattered radiation in GATE were recorded based on the position of source, medical personnel and the position of the patient during the procedure. The beam scattering was measured based on the anterior posterior (AP) exposure projection. In GATE, medical personnel were modelled using a computational International Commission on Radiological Protection (ICRP) 110 phantom, representing an adult reference female. This computational human phantom was employed to evaluate energy deposition across approximately 141 organs resulting from both internal and external radiation exposures. The phantom was developed based on a computed tomography (CT) scan of a 43-year-old individual with a height of 167 cm and a weight of 59 kg. The scan comprised 174 slices of 5 mm thickness for the head and trunk regions, and 43 slices of 20 mm thickness for the legs. Each slice consisting of a (256 × 256) pixel resolution.

Figure 1. Geometries of angiography rooms for simulation **(a)** IR1, **(b)** IR3, **(c)** IR4, **(d)** IR5, **(e)** IR6. The geometries represent different interventional radiology suites within the clinical setting, each with unique room dimensions. These room geometries were modelled based on actual floor plans and equipment layouts to accurately reflect clinical practice and ensure realistic dose estimation using the Monte Carlo GATE simulation framework. (IR 1 (5.75 x 7.00) m, IR 3 (4.55 x 7.70) m, IR 4 (3.89 x 4.57) m, IR 5 (3.43 x 5.76) m, IR 6 (4.22 x 4.65) m measurement).

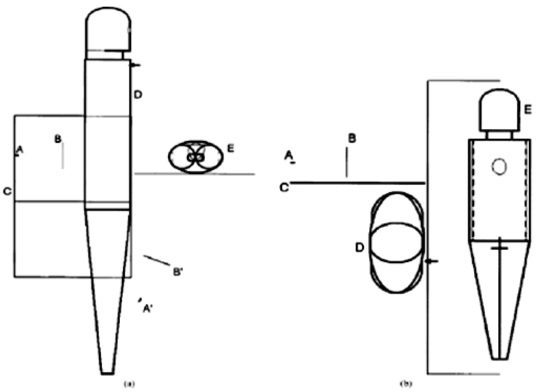

Figure 2. The location of the medical personnel, denoted as D, relative to the patient, represented as E, who is positioned supine on the angiography tabletop. Position D corresponds to the typical standing location of the primary operator (radiologist) during the procedure, often closest to the patient's thoracic region to perform catheter manipulation. The spatial relationship between D and E is critical for accurately assessing occupational radiation exposure in proximity to the X-ray source and patient-scatter field.

[DOI: 10.61186/ijrr.24.3.8]

The three-dimensional voxel array of the computational phantom, organized into columns, rows, and slices, was oriented with the X-coordinates correspond to columns increasing from right to left, the Y-coordinates represent rows increasing from front to back, and the Z-coordinates indicate slices increasing from the toes to the body vertex. This precise anatomical representation facilitated detailed analysis of radiation energy deposition across various organs. Modeled as a rectangle, the phantom representing the patient was based loosely on the Medical Internal Radiation Dose system (MIRD) phantom. Figure 3 illustrates the ICRP and MIRD phantom representing medical personnel in GATE. Table 1 records the main characteristics of the adult female reference computational phantom. Figures 4 illustrates the example of the positions of medical personnel, patient and sources generated in GATE during the intervention procedure.

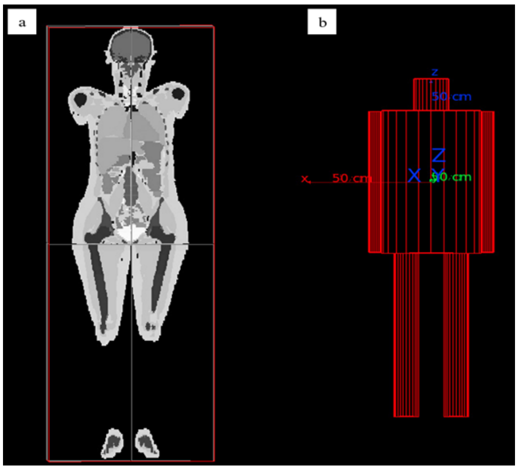

Figure 3. Illustration of **(a)** ICRP phantom and **(b)** MIRD phantom in GATE. ICRP reference computational phantom represents an anatomically realistic male or female adult human body based on medical imaging data. It features detailed organ structures and tissue compositions, allowing for accurate dose estimation aligned with ICRP recommendations. The MIRD phantom depicts a stylized anthropomorphic model with simplified geometries. While less anatomically detailed, it remains widely used for internal dosimetry and comparison studies.

Table 1. Main characteristics of adult female reference computational phantom from ICRP. The phantom is based on voxelized imaging data and represents a standardized adult female with average anatomical dimensions and organ masses, which includes detailed specifications such as body height, weight, organ volumes, and tissue compositions.

Property	Female Reference Phantom
Height (m)	1.63
Mass (kg)	60.0
Number of tissue voxels	3, 886, 020
Slice thickness (voxel height, mm)	4.84
Voxel in-plane resolution (mm)	1.775
Voxel volume (mm^3)	15.25
Number of columns	299
Number of rows	137
Number of slices	346 (+2; additional slices of skin at the top and bottom)

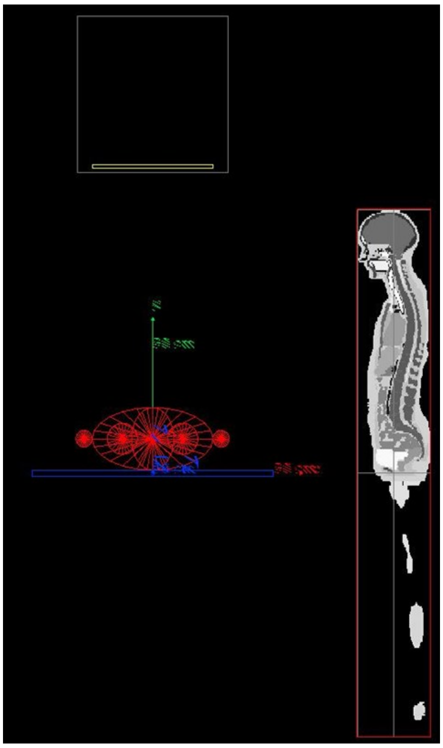

Figure 4. The setup used in the Monte Carlo GATE simulation, showing the relative positions of the key components within the angiography room. The medical personnel, represented by the ICRP reference phantom enclosed in a red box, is positioned adjacent to the patient to reflect a realistic operator stance during the procedure. The patient is shown in solid red, lying supine on the angiographic table in alignment with standard clinical practice. The X-ray detector, highlighted in yellow, is positioned above the patient, mimicking the actual configuration of a flat-panel detector in a C-arm fluoroscopy system.

RESULTS

Generation of geometries in Monte Carlo GATE

The generation of the five angiography room geometries in the Monte Carlo GATE simulation, IR1, IR3, IR4, IR5, and IR6, successfully replicated the typical real-world setting of the spatial configurations and equipment placements of the angiography rooms at the Department of Diagnostic Radiology at Singapore General Hospital, enabling detailed analysis of the radiation exposure patterns. Figure 5 depicts the angiography room geometry generated in GATE. Figure 6 illustrates the spectrum for 73 kVp generated by SpekPy.

Energy spectra generated by SpekPy

The displayed X-ray spectrum represents an X-ray tube operating at 73.0 kVp, illustrating the distribution of X-ray photon fluence (photons/cm^2/mAs/keV) relative to photon energy (keV). Table 2 records the equivalent doses received by several anatomical locations during the procedure for each simulated room.

[DOI: 10.61186/ijrr.24.3.8]

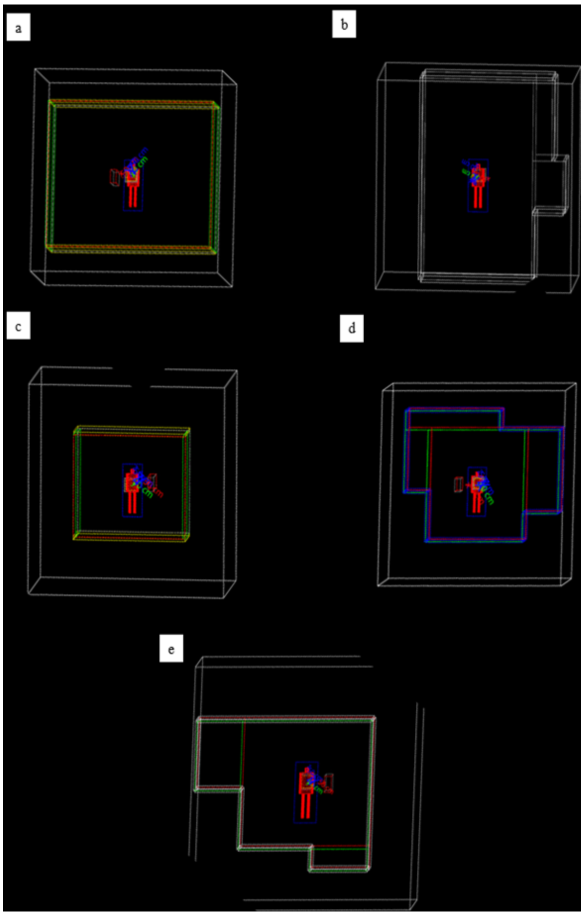

Figure 5. Angiography rooms in GATE **(a)** IR1, **(b)** IR3, **(c)** IR4, **(d)** IR5 and **(e)** IR6. Each room was constructed in GATE based on real clinical floor plans and equipment placements, including the C-arm system and patient table. Variations in room dimensions, wall configurations, and equipment positioning were carefully modelled to assess their impact on radiation dose distribution, particularly in relation to occupational exposure among medical personnel.

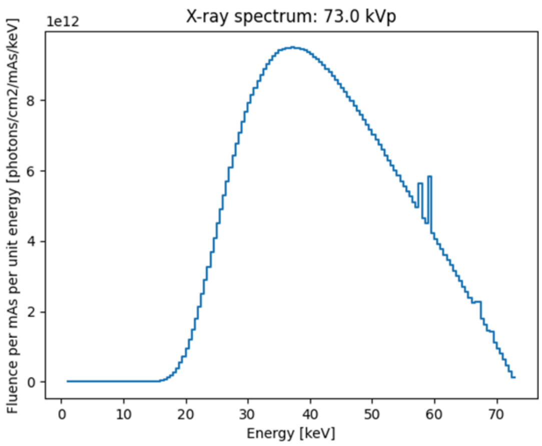

Figure 6. Spectrum for 73 kVp generated by SpekPy. The spectrum reflects the energy distribution of photons emitted from the X-ray tube, incorporating inherent filtration and beam quality characteristics typical of interventional radiology procedures. This input spectrum was used as the primary source definition in GATE simulations to ensure realistic modelling of photon interactions and scatter within the angiography room environment. Accurate representation of the source spectrum is essential for reliable dose calculations, particularly when estimating organ-equivalent doses received by medical personnel.

Table 2. Equivalent doses received by medical personnel in several anatomical locations during the procedure. The dose values reflect occupational exposure under typical clinical conditions and room configurations, providing insight into the distribution and magnitude of radiation dose across the body.

Organ	No room	IR1	IR3	IR4	IR5	IR6
	Dose (µSv)					
Eyes lens (Left)	92.3	276	108	62.3	44.8	92.4
Eyes lens (Right)	122	119	75	147	210	28.8
Gonad (Ovary) Left	122	92.5	88.5	98.8	87.4	93.4
Gonad (Ovary) Right	84.7	83.4	90.3	95.4	86.3	80.6
Skin, arms	101	100	100	100	99.2	101
Thyroid	115	106	109	108	116	115
Uterus/cervix	98.2	102	101	106	99.3	99

Dose measurement in Monte Carlo GATE

Figure 7 presents a comparison of equivalent doses for various organs and body parts across different simulated rooms (IR1, IR3, IR4, IR5, and IR6). The highest doses were often observed for lens, with IR1 exhibiting the greatest dose of 276 µSv for the left lens, followed by contributions of 210 µSv from IR5 with the right lens. The thyroid and uterus/cervix also showed notable exposure across all rooms, with IR6 demonstrating a high thyroid dose of 115 µSv and IR4 demonstrating the highest dose in uterus/cervix of 106 µSv. The gonads received the least exposure across all rooms, with only minimal doses detected ranging from 80.6 to 98.8 µSv, except for room with no specific dimensions. The skin and arms showed moderate exposure, with consistent exposure across the rooms. Overall, the dose distribution varied significantly across different anatomical locations, with IR1 consistently contributing the highest values in most cases, whereas IR6 produced lower doses overall.

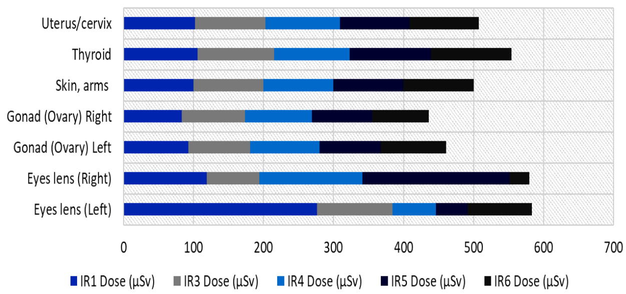

DISCUSSION

In the Monte Carlo GATE simulation, the scattered radiation was meticulously calculated by accounting for the spatial arrangement of key elements during the procedure. This included the precise positions of the radiation source, medical personnel, and patient. The simulation specifically focused on the anterior-posterior (AP) projection, a common and conventional imaging view in diagnostic angiography [23], to model the radiation beam scattering. By simulating this projection, it was possible to analyze how radiation scatters within the environment,

[DOI: 10.61186/ijrr.24.3.8]

considering the geometrical relationship between the source, patient, and medical personnel. This approach provided detailed insights into the distribution of scattered radiation, which is critical for evaluating occupational exposure and enhancing radiation safety protocols in clinical settings.

The X-ray spectrum shown corresponds to an X-ray tube operating at 73.0 kVp. The graph depicts the distribution of X-ray photon fluence (photons/cm^2/mAs/keV) as a function of photon energy (keV). The spectrum exhibits a characteristic Bremsstrahlung radiation, which rises sharply, peaks around 35 to 40 keV, and then gradually decreases towards the maximum energy of approximately 73 keV. Additionally, characteristic X-ray peaks appear around 58 to 62 keV, with previous literature reporting that a Bremsstrahlung peak exists in all clinical X-ray sources at 59 keV (24), likely due to K-shell emissions from the anode material, commonly tungsten (W) or molybdenum (Mo). The overall shape of the spectrum results from electron interactions in the X-ray tube target, where lower-energy photons are more abundant but also more likely to be absorbed by inherent filtration, while higher-energy photons contribute to the useful diagnostic X-ray beam.

The differences in equivalent dose across sensitive organs indicate that highly radiosensitive organs, such as the gonads and eye lenses, are more vulnerable to scattered radiation (25). The heightened exposure in the eye lens, as seen in IR1, emphasizes the importance of dose monitoring in radiation-prone environments to prevent lens opacities and increased risks during lens cataract surgery (26). The discrepancies observed between left and right lens doses may be attributed to variations in radiation interaction and simulation modelling within the GATE framework. Otherwise, the discrepancy may be attributed to the X-ray tube being positioned on the medical personnel's left without adequate ceiling-mounted protection. Previous works also demonstrated that operator position and angulation significantly influence scatter radiation exposure (27–30).

The consistent arm skin dose across all rooms reflects typical hand positioning of medical personnel during the procedure. This dose is clinically relevant as repeated procedures can lead to cumulative hand exposure approaching 500 mSv per year, which is the ICRP annual limit for extremities. To overcome this, (31) previous literature has advocated the use of lead-lined gloves which can reduce the exposure. The hands of medical personnel are often among the most exposed body parts, particularly when working near the primary beam or the patient during a procedure. Lead-lined gloves typically contain specific thickness of lead-equivalent shielding, offering a significant reduction in scatter radiation dose, although they do not provide complete protection.

In radiation transport simulations, slight asymmetries can arise due to statistical uncertainties, voxelized phantom geometry, or differences in the positioning of radiation sources relative to anatomical structures. Uncertainties can also arise from frequent and multiple geometry updates, as well as the configuration of command files (20). Additionally, variations in the relative positioning of the radiation source with respect to the phantom can influence scatter patterns and dose gradients. Even small shifts in source-to-phantom distance and angulation can produce measurable changes in local dose distributions, especially in regions near the field edge or where steep dose gradients are present.

Although the dose measurement is based on the ICRP reference phantom (32), which ensures uniform anatomical composition, discrepancies between the left and right eye lens doses may still arise due to radiation transport physics and simulation settings in GATE. One possible contributing factor is the stochastic nature of Monte Carlo simulations, where statistical fluctuations in photon interactions can produce slight variations in dose distribution, even in symmetric anatomical structures. Additionally, differences in the angle of incident radiation, scattered photon trajectories, and boundary effects within the computational grid can result in asymmetric dose deposition.

The simulations revealed distinct variations in scattered radiation levels across the different room configurations, influenced by factors such as the room structure. Further validation through phantom measurements or real-world clinical comparisons could enhance the credibility of these results. Ultimately, accurate dose simulations are crucial for optimizing radiation protection strategies, ensuring compliance with international safety standards, and minimizing risks to patients and radiation workers.

CONCLUSION

The Monte Carlo GATE simulation provided valuable insights into the distribution of scattered radiation in various room configurations, highlighting the significant exposure to sensitive organs such as the eye lens, particularly in IR1. The results emphasize the vulnerability of highly radiosensitive organs to scattered radiation and the importance of monitoring radiation doses. This signifies the importance of utilizing GATE simulation, as it allows for precise modeling of radiation scattering in different room configurations, leading to accurate dose assessments.

Acknowledgments: The authors thanked the Faculty of Health Sciences, Universiti Kebangsaan Malaysia and Department of Diagnostic Radiology, Singapore

[DOI: 10.61186/ijrr.24.3.8]

General Hospital for allowing this work to be conducted. The authors also acknowledged the Ministry of Higher Education Malaysia for Fundamental Research Grant Scheme (FRGS/1/2019/STG02/USM/02/2) and the Universiti Kebangsaan Malaysia Geran Galakan Penyelidik Muda (GGPM-2023-027) for the financial support.

Funding: This research was supported by the Ministry of Higher Education Malaysia under the Fundamental Research Grant Scheme (FRGS/1/2019/STG02/USM/02/2).

Conflict of Interest: None. The authors declare that they have no known competing financial interests or personal relationships that could have appeared to influence the work reported in this paper.

Ethical Consideration: This study did not involve human or animal subjects and was based entirely on simulation data thus, ethical approval was not required.

Authors' Contribution: M.H. performed the simulations and conducted data analysis and interpretation. Z.S.H. designed the study, wrote, edited and guided in the writing of the manuscript. M.F.R.A.H., M.S.A.F., A. S., N.H.Ab.A., G. R. were involved in data collection and interpretation. All authors reviewed and approved the final manuscript.

AI Usage Declaration: ChatGPT (OpenAI), was used to assist in language editing and formatting.

REFERENCES

1. Sailer AM, Paulis L, Vergoossen L, *et al.* (2017) Real-time patient and staff radiation dose monitoring in IR practice. *Cardiovasc Intervent Radiol*, ***40***:*421-429.*
2. ICRP (2018) Occupational radiological protection in interventional procedures. ICRP publication 139. *Ann ICRP.,* ***47****(2): 1-118.*
3. Mashoufi R and Mashoufi R (2023) Interventional radiology for disease management: A narrative review. *Cureus,* ***15****(11): e48603.*
4. Talapko J, Talapko D, Katalinić D, *et al.* (2024) Health effects of ionizing radiation on the human body. *Medicina (B Aires),* ***60****(4): 653.*
5. Gibb AA, Lazaropoulos MP, Elrod JW (2020) Myofibroblasts and fibrosis: mitochondrial and metabolic control of cellular differentiation. *Circ Res*, ***127****(3): 427-447.*
6. Ejaz A, Greenberger JS, Rubin PJ (2019) Understanding the mechanism of radiation induced fibrosis and therapy options. *Pharmacol Ther*, ***204***:*107399.*
7. Vano E, Sanchez Casanueva R, Fernandez Soto JM, Bartal G (2021) Challenges in occupational dosimetry for interventional radiologists. *Cardiovasc Intervent Radiol.*, ***44****(6): 866-870.*
8. Lee WJ, Bang YJ, Cha ES, Kim YM, Cho SB (2021) Lifetime cancer risks from occupational radiation exposure among workers at interventional radiology departments. *Int Arch Occup Environ Health,* ***94****: 139-145.*
9. Vano E, Kleiman NJ, Duran A, Rehani MM, Echeverri D, Cabrera M (2010) Radiation cataract risk in interventional cardiology personnel. *Radiat Res*, ***174****(4): 490-495.*
10. Machan L. (2018) The eyes have it. *Tech Vasc Interv Radiol*, ***21****(1): 21-25.*
11. Matuszak N, Piotrowski I, Kruszyna-Mochalska M, Skrobala A, Mocydlarz-Adamcewicz M, Malicki J (2024) Monte Carlo methods to assess biological response to radiation in peripheral organs and in critical organs near the target. *Reports Pract Oncol Radiother J Gt Cancer Cent Pozn Polish Soc Radiat Oncol.*, ***29****(5): 638-648.*
12. Khosravi H, Ghazikhanlu sani K, Jafari S, Nikzad S (2023) Evaluation of the radiation protection capability of a low density and non-Lead composite shield using Monte Carlo model TT. *Int J-Radiat Res*, ***21****(4): 833-836*.
13. Kholghi N, Pouladian M, Shabestani Monfared A (2023) Modification of binomial lateral spreading function for oblique electron beams in pencil beam algorithm based on Monte Carlo simulations TT. *Int J Radiat Res*, ***21****(4):789-795.*
14. Herwiningsih S and Fielding AL (2023) Monte Carlo simulation for verification of lung stereotactic treatment plans delivered with an Elekta beam modulator collimator systems TT. *Int J Radiat Res ,* ***21*** *(4):757-764.*
15. Yeke Dehghan AB, Mostaar A, Azadeh P (2023) Implementation of geant4 application for tomography emission Monte Carlo Code in the calculation of dose distribution in external radiation therapy TT. *Int J Radiat Res*, ***21****(4): 663-673*.
16. León MI, Quispe B, Gutiérrez L, *et al.* (2024) Eye lens dose estimations in chest computed tomography examinations using Monte Carlo simulations in a Siemens SOMATOM perspective scanner TT. *Int J Radiat Res,* ***22****(4): 853-860.*
17. Qomariyah N, Haryanto F, Waris A, Wirawan R (2025) Investigation of the effects of tissue material on the energy spectrum from Bebig Co-60 High Dose Rate Brachytherapy source based on the Monte Carlo simulation TT. *Int J Radiat Res*, ***23****(1): 97 -102*.
18. Talebi AS and Rajabi H (2024) Spread-out of Bragg peak of proton beam using Au nanoparticles: A Monte Carlo simulation study TT. *Int J Radiat Res*, ***22****(3): 697-701.*
19. Zuber SH, Abdul Hadi MFR, Hashikin NAA, *et al.* (2022) Estimation of linear and mass attenuation coefficients of soy–lignin bonded Rhizophora spp. Particleboard as a potential phantom material using caesium-137 and cobalt-60. *Radiat Environ Biophys*, ***61****(3): 435-443.*
20. Zuber SH, Hadi MFRA, Samson DO, *et al.* (2023) Dosimetric Analysis of Rhizophora-based Phantom Material in Radiation Therapy Applications Using Monte Carlo GATE Simulation. *J Med Phys*, ***48****(4): 358-364.*
21. Zuber SH, Hadi MFRA, Hashikin NAA, *et al.* (2025) Dosimetric evaluation of brain radiotherapy using custom-made Rhizophora head phantom–comparison between Monte Carlo GATE and treatment planning system MONACO. *Int J Radiat Res*, ***23****(1): 13-20.*
22. Binti Zuber SH, Hadi MFRA, Hashikin NAA, Yusof MFM, Aziz MZA (2024) Rhizophora-based particleboard bonded with soy flour and lignin as potential phantom. *BioResources*, ***19****(3): 5467-5482.*
23. Di Mario C and Sutaria N (2005) Coronary angiography in the angioplasty era: projections with a meaning. *Heart*, ***91****(7): 968-976*.
24. Nan W, Zhang L, Li S, *et al.* (2024) Achieving Ultrahigh Photoluminescence Quantum Yield in Highly Stable Cs3Cu2I5 Perovskite Single Crystals Through Melt Growth. *Inorg Chem*, ***63*** *(50): 23691-23697.*
25. Wang WH, Wei KC, Huang WC, Yen YY, Mar GY (2021) Radiation reduction and protection for radiosensitive organs (Lens, thyroid, and genital organs) of patients receiving percutaneous coronary intervention-real-world measurement of radiation dose in a single center. *J Cardiovasc Dev Dis*, ***8****(8).*
26. Wei KC, Bee YS, Wang WH, Huang YT, Lu TH (2016) Incidence of cataract surgery in patients after percutaneous cardiac intervention in Taiwan. *JAMA Intern Med*, ***176****(5): 710-711.*
27. Shikhar A, Akhil P, Singh BN, *et al.* (2014) Relationship of Beam Angulation and Radiation Exposure in the Cardiac Catheterization Laboratory. *JACC Cardiovasc Interv*, ***7****(5): 558-566*.
28. Haqqani OP, Agarwal PK, Halin NM, Iafrati MD (2012) Minimizing radiation exposure to the vascular surgeon. *J Vasc Surg*, ***55****(3): 799 -805*.
29. Leyton F, Nogueira MS, Gubolino LA, Pivetta MR, Ubeda C (2016) Correlation between scatter radiation dose at height of operator's eye and dose to patient for different angiographic projections. *Appl Radiat Isot*, ***117****: 100-105.*
30. Roh Y, Kim J, Park H, Kim J, Ryu D, Chun K, Yoon Y (2021) Effect of exposure angulation on the occupational radiation exposure during cardiac angiography: simulation study. *International journal of environmental research and public health,* ***18****(15), 8097.*
31. Lipsitz EC, Veith FJ, Ohki T (2010) Reducing radiation exposure during endovascular procedures. *Endovasc Surg E-b Expert Consult Print, with Video*, ***500****: 41*.
32. Menzel HG, Clement C, DeLuca P (2009) ICRP Publication 110. Realistic reference phantoms: an ICRP/ICRU joint effort. A report of adult reference computational phantoms. *Ann ICRP*, ***39****(2): 1-164.*

[DOI: 10.61186/ijrr.24.3.8]